Preprints, 4th IFAC Conference on
Advances in Proportional-Integral-Derivative Control
Almería, Spain | June 12-14, 2024

PID Control of DC Actuators. Consideration to Energy Robotic Design

Antonio Garcia-Chica * **Jose L. Torres-Moreno** *
Antonio Gimenez *

* *Dpto. de Ingeniera, Universidad de Almería – CIESOL, Almeria, 04120 Spain (e-mail: agc989@inlumine.ual.es).*

Abstract: This works proposes a robot control architecture combining a PID position controller and a PI current controller, which is experimentally validated by using a tested including a DC motor and a high inertia load. Once the architecture is validated, it is used to address a performance comparison between series robots and parallel robots for a given task. In view of the obtained results, it is shown that the parallel configuration may lead to considerable energy savings with respect to the serial configuration.

Keywords: Application of mechatronic principles, Mechatronic systems, Modeling, Motion Control Systems, Robots manipulators.

1. INTRODUCTION

Currently, robots are applied in a wide variety of fields such as computing, electronics, mechanics industry. These robots known as manipulator robots are intended for the manipulation of objects, performing different types of actions or activities depending on the tool placed at their end, the end effector, and the programming. Since its implementation in the industry, great improvement has been achieved in production, achieving work done more quickly and accurately compared to human labour, and providing safety in activities, avoiding occupational risks for workers Villani et al. (2018). Robots are formed by the combination of links and joints, adopting different configurations form different types of robot applications. This article deals with both serial robots and parallel robots. Serial robots are robotic arms that have joints connected in series, each joint being one or more motors or actuators, while parallel robots are those that are composed of a fixed base connected to a mobile platform through two or more closed kinematic chains Siciliano et al. (2010). In each case, inverse kinematics algorithms are implemented. This way, the position and orientation of the end effector determine the coordinates of the robot joints and hence the DC actuator setpoints.

Position control of the motors associated with the joints of a robot is typically performed through PID control. In most of the works found in the literature, control schemes are presented that assume that the torque resulting from the control action can be provided instantaneously, as in Perrusquia et al. (2020). Other works present control schemes that do take into account the dynamics of the control driver but focus on voltage regulation Orrante-Sakanassi et al. (2013). However, to the best of the authors' knowledge, we have not found works that combine the position control of the robot together with the current control of the driver together with the dynamics of the robot.

Therefore, in this work, we take these aspects into account and propose a combined DC actuator control model including the dynamics of the driver and the robot to carry out a comparative analysis between a series robot and a parallel robot configuration performing similar tasks. For this purpose, the modelling of a DC motor and its corresponding control unit is carried out, which implements a double control loop. This double control loop consists of a current PI controller and a position-feedforward PID controller. The rest of the article is structural as follows: Section 2 shows the modelling of the motor and validation of the control unit, section 3 explains the modelling of a Robot with Two Degrees of Freedom, section 4 shows the results of the two proposed robot configurations and section 5 shows the conclusions.

2. MODELLING OF THE MOTOR AND DRIVER

In robot construction, it is common to use gears to amplify the motor torque or use screw spindles to convert the rotational movement of the motor into linear displacement. The inherent flexibility and looseness of these parts generate an elasticity phenomenon, along with a delay in the transmission chain Fareh et al. (2021). In many cases, the mechanical connection between the motor and the load also has some backlash, which causes a delay in the system, Memar and Esfahani (2016). This delay influences regulation and has a significant impact, as it decreases dynamic responsiveness and control precision, so a PID controller is always necessary for these robots.

To correct these limitations and combine a motor-load system with precise dynamic regulation, it is necessary to control the motor motion, including the load. For this purpose, a control architecture is proposed with a main PID controller and a secondary current PI controller, which is shown in Fig. 1.

To verify this control system of two controllers, a test is proposed in which experimental validation of the the-

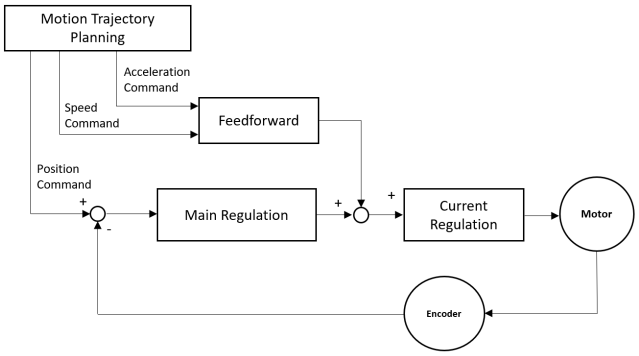

Fig. 1. Control loop including position and current regulation

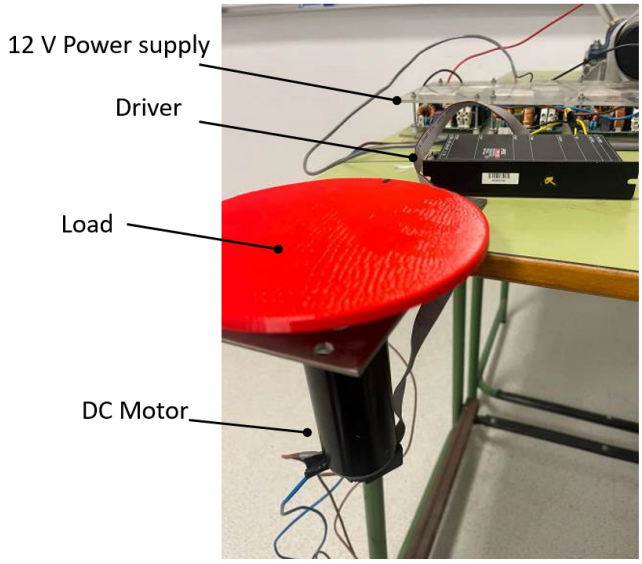

Fig. 2. Experimental testbed

oretical model of a high inertia and low friction system is sought. For this purpose, a testbed composed of a motor with encoder connected to an inertia disc This testbed is shown in Fig. 2, whose parameters are summarised in table 1. The DC motor model is Maxon EC 40, and the encoder is HEDL 5540, whereas the driver is the Controller EPOS2 70/10.

Table 1. Motor parameters

	Description	Value	Units
n_0	No load speed	5950	rpm
I_0	No load current	236	mA
I_n	Nominal current	10.8	A
R	Resistance phase to phase	0.103	Ω
L	Inductance phase to phase	0.0717	mH
k_M	Torque constant	38.5	nNm/A
J_{mot}	Rotor inertia	536	gcm^2
J_{load}	Load inertia	5000	gcm^2
p	Encoder pulses per rev.	500	ppr

To validate the experimental model, a dynamic model has been implemented in Simulink. In this model, the input instructions are presented where the desired position is sent, as well as the maximum allowed speed and acceleration. The two controllers, a PID controller, and a PI controller are also introduced to regulate the current.

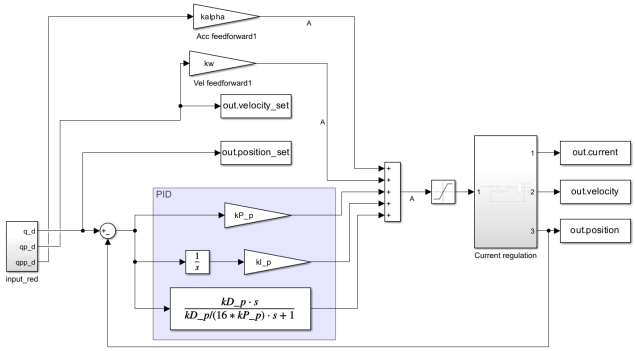

Fig. 3. Control loop used in the testbed

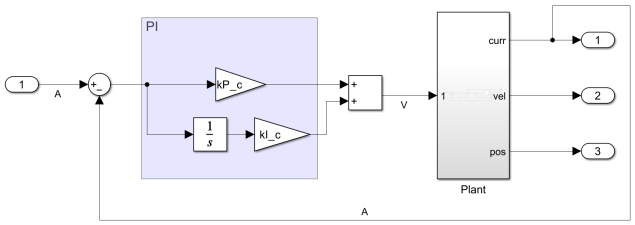

Fig. 4. Current control subsystem

In this type of system, the non-linearities of the reducers and the static and dynamic frictions produced in each of the joints cause the need to have pre-feeding, Ogata (2009), as shown in Fig. 3. As can be seen, the main controller consist of a PID controller with feedforward, while Fig. 4 shows the secondary control system made up of a PI controller.

The experiment is configured as follows: A trapezoidal signal has been configured with maximum speed of 31.42 rad/s and maximum acceleration of 78.54 rad/s^2 so the disk rotates 5000 qc in 1 s. In addition, current, position and velocity are registered with a fixed sample time of 13.7 ms. The results of the experiment are shown in Fig. 5.

As can be seen, Fig. 5c shows that the disk position fits the requirements whereas Fig. 5b shows that the velocity constraints are accomplished. Finally, the current consumption is shown in Fig. 5a, where the accuracy of the electrical model of the DC motor is demonstrated.

3. MODELLING OF A TWO DEGREES OF FREEDOM ROBOT

In this section, the previously developed motor and control unit model will be used for the sizing of a two-degree-of-freedom manipulator robot. The intended use of this robot consists of performing pick and place functions, with an estimated load of 5 kg, and a minimum range of between 0.5 m and 1 m from the base. (i) A series robot composed of two links, actuated by a DC motor located at the beginning of each link, as shown in Fig. 6a. (ii) A parallelogram-type parallel robot, with the motors located at the base, as shown in Fig. 6b.

In both cases, the same DC motors and the control unit whose models were validated in previous section will be used, with the incorporation of a 1:100 reduction planetary-type reducer. Taking this into account, it is possible to relate the torques provided by the motor with

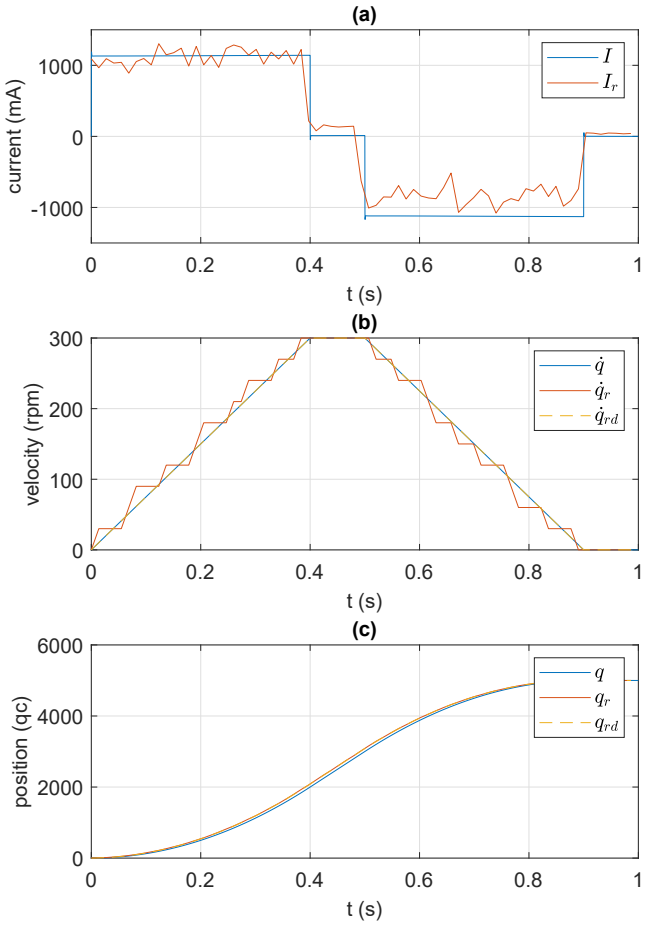

Fig. 5. Model validation. (a) Simulated current, I, and measured current, I_r. (b) Simulated velocity, $\dot{q}$, measured velocity, $\dot{q}_r$, and velocity setpoint, $\dot{q}_{rd}$. (c) Simulated position, q, measured position, q_r, and position setpoint, q_{rd}.

the performance of the robots through its dynamic model, represented by the following equation:

$$\tau = \mathbf{M}(\theta)\ddot{\theta} + \mathbf{C}(\theta, \dot{\theta}) + \mathbf{G}(\theta) + \mathbf{f}(\dot{\theta}). \quad (1)$$

Where $\mathbf{M}$ is the inertia matrix, $\mathbf{C}$ is the matrix of centrifugal and Coriolis forces, $\mathbf{G}$ is the matrix of gravitational forces, and $\mathbf{f}$ represents the friction term. It is worth mentioning that, in the case of the parallel robot, there are also two degrees of freedom due to the relationship between the independent coordinates associated with the motors θ and the dependent coordinates associated with the rest of the joints θ', through the following expression:

$$\theta' = \sigma(\theta). \quad (2)$$

where the sigma function represents the kinematic position problem of the associated mechanism Siciliano et al. (2010).

In order to perform the experiments and compare the dynamic behaviour of both options, a simulator has been developed that combines the DC motor model developed in the previous section, with the dynamic model represented by "(1)" and "(2)", which is implemented using the Simescape Multibody tool, due to its suitability for this kind of simulations, Torres-Moreno et al. (2023). A general schematic of the simulator can be seen in Fig. 7.

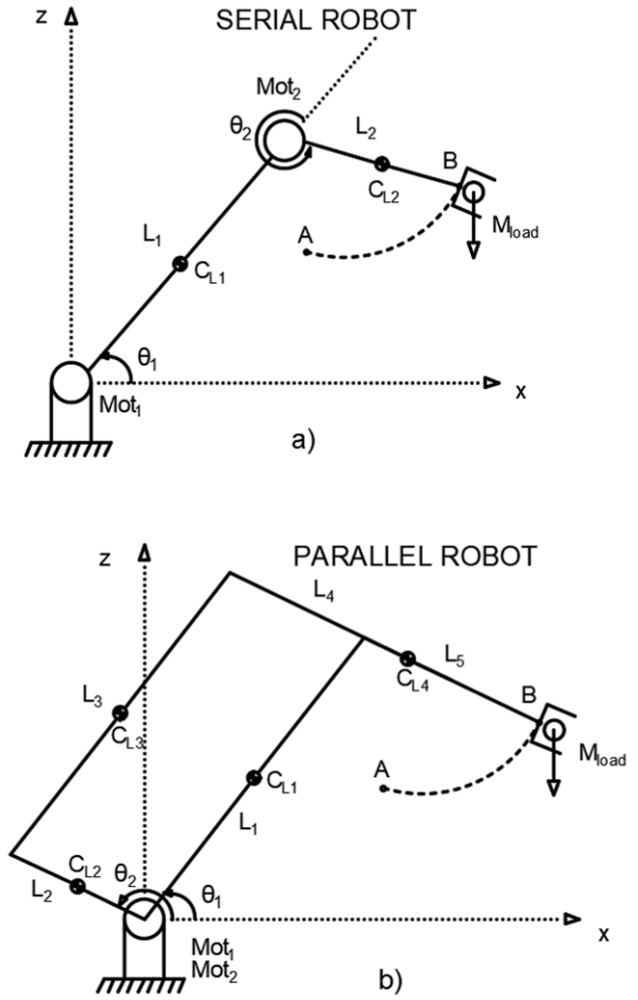

Fig. 6. Schematics of the considered robots: (a) Serial Robot (b) Parallel Robot.

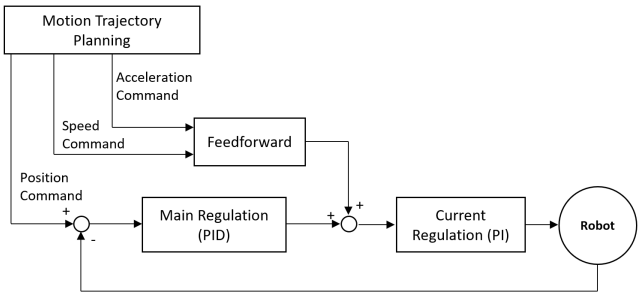

Fig. 7. Control system implemented in the robot simulations

As can be seen, the desired position, speed, and acceleration setpoints are entered, and the controllers calculate, first, the necessary torques, and second, the current to be provided by the power stages (drivers), while at the same time The direct dynamic model of the robot allows the reading of the position reached by the links that compose it.

4. RESULTS

To determine which configuration is most appropriate, a trajectory is made that adapts to the operations for which

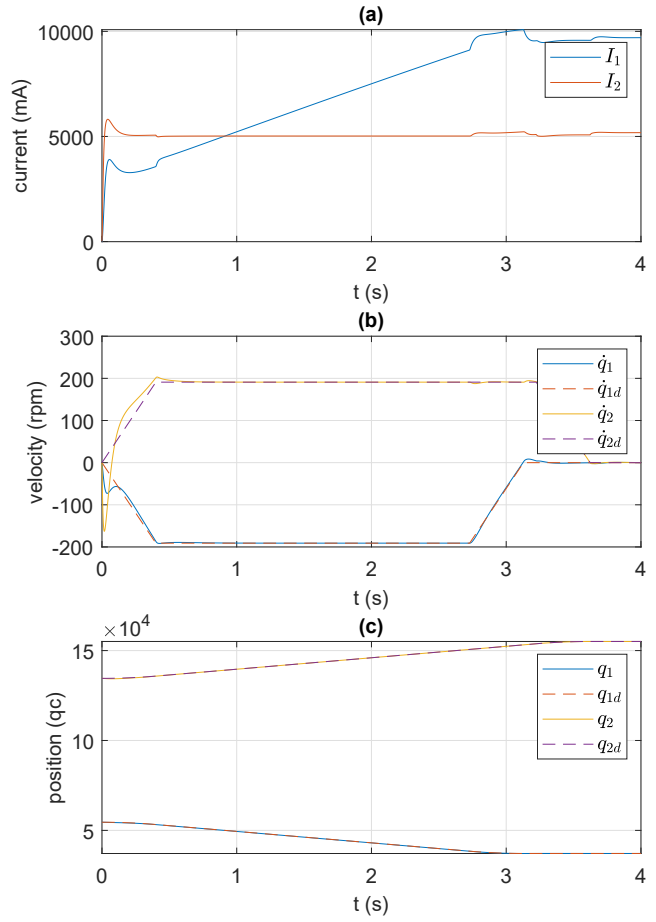

Fig. 8. Current, velocity, and position results of the experiment with the serial configuration.

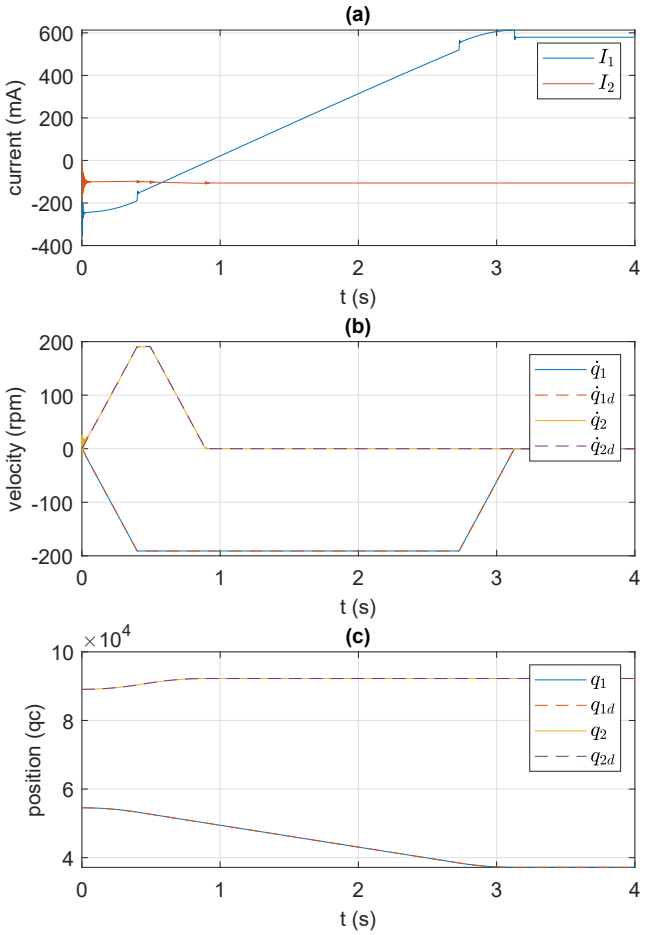

Fig. 9. Current, velocity, and position results of the experiment with the parallel configuration.

the robot will be designed, consisting of transferring the 5 kg load from the Cartesian coordinates X=0.3, Z=0.4 that correspond to the joint coordinates of the series robot (θ_1 = 1.713 rad and θ_2 = 4.226 rad) and of the parallel robot (θ_1 = 1.713 rad and θ_2 = 2.798 rad) to the Cartesian coordinates X=0.6, Z=0.4 that correspond to the joint coordinates of the series robot (θ_1 = 1,167 rad and θ_2 = 4,871 rad) and the parallel robot (θ_1 = 1,167 rad and θ_2 = 2,897 rad). Serial robot main parameters are listed in table 2, whereas parallel robot main paramenters are listed in table 3.

Table 2. Serial robot parameters

	Description	Value	Units
L_1	Length L_1	0.54	m
L_2	Length L_2	0.4	m
C_{L_1}	Center of mass L_1	0.27	m
C_{L_2}	Center of mass L_2	0.2	m
M_{load}	Weight of the load	5	kg
M_{mot}	Weight of the DC motor	2.64	kg
M_{L_1}	Weight of L_1	0.54	kg
M_{L_2}	Weight of L_2	0.4	kg
I_{c_1}	Inertia of L_1	0.0131	kgm^2
I_{c_1}	Inertia of L_2	0.0053	kgm^2

As a measure of performance, we will focus on the current consumption of the motor control units in both configurations, rewarding the configuration that has the lowest consumption, Soori et al. (2023). First, the results corresponding to the series robot are shown. The trajectory carried out in the joint space corresponds to a trapezoidal velocity profile motion, as shown in Fig. 8b, and a motion of the robot from position A to position B, as shown in Fig. 8c. Finally, Fig. 8a shows the current used by the motors. As can be seen, maximum values of 10 A are reached, which correspond to the maximum torque that motor 1 must provide. In the most unfavourable position of the arm, that is, at its greatest extension.

Table 3. Parallel robot parameters

	Description	Value	Units
L_1	Length L_1	0.54	m
L_2	Length L_2	0.125	m
L_3	Length L_3	0.54	m
L_4	Length L_4	0.125	m
C_{L_1}	Center of mass L_1	0.27	m
C_{L_2}	Center of mass L_2	0.0625	m
C_{L_3}	Center of mass L_3	0.27	m
C_{L_4}	Center of mass L_4	0.0625	m
M_{load}	Weight of the load	5	kg
M_{L_1}	Weight of L_1	0.54	kg
M_{L_2}	Weight of L_2	0.0125	kg
M_{L_3}	Weight of L_3	0.154	kg
M_{L_4}	Weight of L_4	0.525	kg
I_{c_1}	Inertia of L_1	0.0131	kgm^2
I_{c_2}	Inertia of L_2	0.000162	kgm^2
I_{c_3}	Inertia of L_3	0.0131	kgm^2
I_{c_4}	Inertia of L_4	0.000683	kgm^2

Secondly, the results corresponding to the parallel robot are shown. The trajectory carried out in the joint space follows a trapezoidal velocity profile, as shown in Fig. 9b, from position A to position B, as shown in Fig. 9c. Finally, Fig. 9a shows the current used by the motors. As can see seen, peak values of only 0.6 A are reached, which correspond to the maximum torque that motor 1 must provide, in the most unfavourable position.

5. CONCLUSION

The article can be concluded by stating that the proposed control system with double PID and PI controller has been experimentally validated with a motor coupled to a high inertia load.

In addition, it has been demonstrated the importance of the moments of inertia of the loads, the effect of gravity, and the coupling of reducers when designing a robot. These parameters significantly influence the torque that robot motors must produce. In the analysis carried out, it is clearly observed in Figures 8a and 9a that for the same displacement of a load, serial robot current consumption maybe up to 9.4 A greater than a parallel robot.

REFERENCES

Fareh, R., Khadraoui, S., Abdallah, M.Y., Baziyad, M., and Bettayeb, M. (2021). Active disturbance rejection control for robotic systems: A review. *Mechatronics*, 80, 102671. doi: https://doi.org/10.1016/j.mechatronics.2021.102671.

Memar, A.H. and Esfahani, E.T. (2016). Modeling and dynamic parameter identification of the schunk powerball robotic arm. *Proceedings of the ASME Design Engineering Technical Conference*, 5C-2015. doi: 10.1115/DETC2015-47703.

Ogata, K. (2009). Modern control engineering. *Pearson*, 922.

Orrante-Sakanassi, J., Santibañez, V., and Moreno-Valenzuela, J. (2013). Stability analysis of a voltage-based controller for robot manipulators. *International Journal of Advanced Robotic Systems*, 10. doi: 10.5772/53894.

Perrusquia, A., Flores-Campos, J.A., and Torres-San-Miguel, C.R. (2020). A novel tuning method of pd with gravity compensation controller for robot manipulators. *IEEE Access*, 8, 114773–114783. doi: 10.1109/ACCESS.2020.3003842.

Siciliano, B., Lorenzo, S., Villani, L., and Orilo, G. (2010). *Robotics: Modelling, Planning and Control.*

Soori, M., Arezoo, B., and Dastres, R. (2023). Optimization of energy consumption in industrial robots, a review. *Cognitive Robotics*, 3, 142–157. doi: 10.1016/J.COGR.2023.05.003.

Torres-Moreno, J.L., Blanco-Claraco, J.L., and Gimenez-Fernandez, A. (2023). General-purpose software tools in teaching mms. *Mechanisms and Machine Science*, 128, 201–211.

Villani, V., Pini, F., Leali, F., and Secchi, C. (2018). Survey on human–robot collaboration in industrial settings: Safety, intuitive interfaces and applications. *Mechatronics*, 55, 248–266. doi: https://doi.org/10.1016/j.mechatronics.2018.02.009.